LA-UR- 92-756

Los Alamos National Laboratory is operated by the University of California for the United States Department of Energy under contract W-7405-ENG-36

TITLE: ON THE HOT-SPOT-CONTROLLED CRITICAL HEAT FLUX MECHANISM IN POOL BOILING OF SATURATED FLUIDS

LA-UR--92-756

DE92 011352

AUTHOR(S): C. Unal
P. Sadasivan
R. A. Nelson

SUBMITTED TO: The Engineering Foundation Conference on Pool and External Flow Boiling
March 22–27, 1992
Santa Barbara, CA

Los Alamos National Laboratory
Los Alamos, New Mexico 87545

LA-UR-92-R132

ON THE HOT-SPOT-CONTROLLED CRITICAL HEAT FLUX MECHANISM IN POOL BOILING OF SATURATED FLUIDS

by

Cetin Unal, Pratap Sadasivan, and Ralph A. Nelson

Los Alamos National Laboratory
Nuclear Technology and Engineering Division
Engineering and Safety Analysis Group
Los Alamos, NM 87545

ABSTRACT

In this paper, we further investigate the hypothesis that the critical heat flux (CHF) occurs when some point on the heated surface reaches a high enough temperature that liquid can no longer contact that point, resulting in a gradual but continuous increase in the overall surface temperature. This hypothesis unifies the occurrence of the CHF and the quenching of hot surfaces by relating both to the same concept, i.e., the ability of a liquid to contact a hot surface.

We use a two-dimensional transient conduction model to study the boiling phenomenon in the second transition region of saturated pool nucleate boiling on a horizontal surface. The heater surface is assumed to consist of two regions: a dry patch region formed as a result of complete evaporation of the thinner liquid macrolayers and a two-phase macrolayer region formed by numerous vapor stems penetrating relatively thick liquid macrolayers. The constitutive relations used to determine the stem-macrolayer configuration in the two-phase macrolayer region of the boiling surface were reevaluated for Gaertner's clean water and water-nickel/salt solution.

Based upon the conclusions obtained in the previous study of Unal et al. (1991), it was assumed that a stationary, circular, dry patch occurred instantaneously on the heater surface at the beginning of each vapor mushroom period. Therefore, no heat transfer is considered in the dry portion of the heater. Using the information provided by Gaertner (1965) for the second transition region, the liquid-solid contact temperature at the center of dry patches was found to vary from 268°C to 179.7°C for Gaertner's clean water and water-nickel/salt solutions, which were estimated to have contact angles of 90° and 12°, respectively. The size of the dry patch increased with decreasing contact angle. The calculated contact temperatures were in reasonable agreement with the liquid-solid contact temperatures at the onset of film boiling reported by Ramilison and Lienhard (1987). This suggested that the controlling mechanisms for the CHF and quenching could be similar, i.e., they are both dictated by the ability of liquid to contact a hot surface. The occurrence of such a hot spot on the surface appears to be the real cause of CHF.

Possible reasons why CHF was observed at lower heat fluxes in some pool boiling studies were also investigated. Data reported by Wang and Dhir (1991) were studied to address this issue. It was concluded that the critical solid-liquid contact temperature could be reached at lower CHF values depending upon the number of active nucleation sites.

I. INTRODUCTION

Although boiling heat transfer offers a very effective way of transporting of high thermal energies from power-generating equipment, the lack of complete understanding of the heat transfer mechanism near the first boiling crisis (critical heat flux, CHF) prevents designers from obtaining maximum efficiency while retaining the necessary margins of safety. The development of new technologies or

better use of existing technologies will strongly depend on development of mechanistic models for the heat-transfer process near CHF.

Previous studies of the critical heat flux in pool boiling can be classified in four major categories: (1) empirical correlations, (2) bubble interaction models, (3) hydrodynamic instability models (Hsu and Graham 1976), and (4) surface-controlled CHF models (Unal et al. 1991). For the empirical models (Kutateladze 1951, Sterman 1953, and Borishansky 1965), the CHF is expressed in terms of dimensionless groups and either a statistical fit or a fit based upon some simple model is obtained. Bubble interaction models (Rohsenow and Griffith 1956, and Chang and Snyder 1960) consider the CHF to be limited by the removal rate of bubbles, which carry away the heat in the form of evaporation. This theory was based on critical bubble spacing near the heated surface. The hydrodynamic model based on the instability of a wave at the liquid-vapor interface was first proposed by Chang (1957), but it was completed by Zuber (1958, 1959, 1961). This approach assumes that near the CHF point, the heating surface is covered by rising vapor columns with counter-current liquid jets flowing downward to replenish the evaporation loss. When the relative velocity is high enough, an instability (Kelvin-Helmholtz) occurs and the vapor jets collapse. This collapse produces the CHF condition by preventing the escape of the vapor, and because the surface is vapor covered, the return of liquid to the surface. Although Zuber's instability theory is significant and superior to the others, it does not consider the effect of heater geometry and surface conditions mechanistically.

The existence of a thin liquid macrolayer on the heated surface with many vapor stems observed by Kirby and Westwater (1965) and by Yu and Mesler (1977) initiated the development of surface-controlled CHF models. Haramura and Katto (1983) postulated that CHF will occur if the heat flux is high enough to evaporate a thin layer of liquid, assumed to exist between the vapor mass and the heater surface, before the vapor mass (mushroom) leaves the surface. In Unal et al. (1991), we

investigated the hypothesis that there should be another condition for the occurrence of CHF, in addition to the complete evaporation of the liquid macrolayer before vapor mushroom departure—namely, some point on the heater surface must reach a temperature high enough that liquid can no longer contact that point. This hypothesis might be considered as a simple extension of Katto's CHF theory and unifies the occurrence of CHF and the quenching of hot surfaces to the same concept, i.e., the ability of a liquid to contact a hot surface.

Once this "hot-spot" condition occurs at a local point within the dry patch on the heater surface, the further response of the surface depends upon the heater/boiling system's stability as defined by Hesse (1973) and the test procedure used if the system is power controlled. Conceptually for "ideal" temperature-controlled systems, all increasingly higher temperatures above CHF are stable and data can be obtained. Depending upon the system's thermal resistance, power-controlled systems may also have stable transition boiling regions that the experimenter can realize if he "gently moves" the system into transition boiling by decreasing the heat flux as the temperature rises. If the experimenter does not decrease the power or the system is simply unstable in the transition boiling regime, the hot spot begins to grow, further deteriorating the heat removal and increasing the average wall temperature for each bubble in a transient process until the next stable film boiling point is reached.

In Unal et al. (1991), we investigated the feasibility of the hot-spot hypothesis for the occurrence of CHF by examining the second transition (dry patch) region observed experimentally by Gaertner and Westwater (1960) and Gaertner (1965). A two-dimensional transient conduction heat-transfer model was developed to investigate the heat-transfer mechanism. The initial macrolayer thickness on the dry portion of the heater, in the second transition region, was found to be bounded between zero and a maximum thickness of 11 μ for a copper heater. Reasonable

liquid macrolayer thickness were thought to be around 4 to 8 μ. This implies that the formation of liquid macrolayers in the dry patch areas can not be controlled by the Helmholtz hydrodynamic instability mechanism because that approach predicts much thicker liquid macrolayers. The mechanism responsible for the formation of thinner macrolayers in localized areas could be due to the hydrodynamics of the departing vapor mushroom controlling the amount of liquid resupply to the heated surface and the local surface nucleation characteristics.

It was found that the critical liquid-solid contact temperature at the onset of CHF (the surface temperature at the center of the dry patch) must be smaller than the homogeneous nucleation temperature of the liquid for the pool boiling of water on a horizontal clean surface. The liquid-solid contact temperature was dependent upon the initial liquid macrolayer thickness, varying from 180°C to 157°C, for the bounding initial macrolayer thicknesses of 0 and 11 μ, respectively. These values were found to be in good agreement with extrapolated contact temperature data at the onset of film boiling reported by Ramilison and Lienhard (1987). This indicated that the mechanism for the occurrence of the CHF could be similar to the mechanism generally accepted for the quenching of hot surfaces.

In that study, we used Gaertner's pool boiling data for clean water only and assumed that the contact angle of water on copper surfaces was around 90°. This assumption was based upon Liaw and Dhir's (1989) contact angle measurements for a similar heater-liquid combination. Thus, the liquid-solid contact (rewetting) temperature at the onset of CHF was only calculated for one contact angle. Gaertner and Westwater (1960) also reported pool boiling data for water-nickel/salt solutions on horizontal copper surfaces. These data were the first to be reported on the existence of a second transition region in the nucleate boiling region of the boiling curve. Although, the value of CHF was not very much different from that of the water data, the surface-time-averaged (STA) wall temperature at CHF was 121.6°C,

significantly higher than the corresponding value for water, 43.5°C. This can be seen in Fig. 1. The contact angle of the water-nickel/salt solution was unknown to us at the time we did our analysis. Therefore, we did not use water-nickel/salt data in our previous analysis.

Recently, Wang and Dhir (1991) obtained very valuable pool boiling data for water on a vertical copper surface, including the variation of the number of active sites with heat flux for different contact angles. They concluded that the contact angle of the water-nickel/salt solution used by Gaertner and Westwater was less than 18°. Thus, in this paper, we further extended the hot-spot-controlled CHF analysis to the lower contact angles and reanalyze Gaertner's water and water-nickel/salt pool boiling data shown in Fig. 1. The first objective is to test the hot-spot hypothesis further in the light of this additional data, and to confirm the functional variation of the critical rewetting temperature with the contact angle.

Further, the two data sets of Gaertner and Wang and Dhir are plotted in Fig. 2. Two significant differences can be noted between the data sets. The first difference is the absence of a second transition in the data of Wang and Dhir. The second difference is a significant drop in the CHF value with increasing contact angle for the data of Wang and Dhir. If the hot-spot CHF model is to be a viable model explaining the phenomena, it must be able to offer an explanation for both of these difference. Thus, the second objective of this paper is to further investigate these two differences within the frame work of the hot-spot model.

To assist the reader, the following nomenclature is used in the paper.

NOMENCLATURE

c Specific heat capacity

h Heat-transfer coefficient

H	Heater thickness
k	Thermal conductivity
LP	Integer defining the heat flux boundary condition
N/A_w	Nucleation site density
r	Space coordinate
Q_o	Heat generation
q	Heat flux
t	Time
T	Temperature
z	Space coordinate
ΔT_{BL}	Wall superheat at the bottom-left corner of the heater at the end the lifetime of the vapor mushroom (see Fig. 3a)
ΔT_{BR}	Wall superheat at the bottom-right corner of the heater at the end of the lifetime of the vapor mushroom (see Fig. 3a)
ΔT_{TL}	Wall superheat at the top-left corner of the heater at the end of the lifetime of the vapor mushroom (see Fig. 3a)
ΔT_{TR}	Wall superheat at the top-right corner of the heater at the end of the lifetime of the vapor mushroom (see Fig. 3a)
θ	Contact angle
δ	Macrolayer thickness
Δ	$T - T_{sat}$
ρ	Density
τ	The lifetime of the vapor mushroom (hovering period)
$n\tau$	The number of hovering periods
$< >$	Time dependent, surface averaged

Subscripts

av	Surface-time average
CHF	Critical heat flux
d	Dry patch
h	Heater
hn	Homogeneous nucleation
rew	Rewetting
s	Stem
sat	Saturation
1	Dry patch region
2	Two-phase macrolayer region

II. THE HEAT-TRANSFER MODEL

In this section, we will summarize the main features of the heat-transfer model used in this paper. Complete details of the model were previously discussed in the paper by Unal et al. (1991). The focus is the investigation of the boiling phenomena near the boiling crisis on a microscopic transient level.

A key assumption we make for this analysis is that CHF is independent of the boiling surface orientation—Gaertner used a horizontal heater, while Wang and Dhir employed a vertical heater. The results of Nishikawa et al. (1984) clearly show that changes in heater surface orientation do not cause any significant change in the boiling characteristics for the fully developed, high heat flux, nucleate boiling region. Thus for a given heat flux, the same wall superheat results for horizontal and vertical surfaces. Unfortunately, Nishikawa et al. do not indicate if CHF does or does not vary for the different orientations. The only information of which we are currently aware that does give some indication of this type variation is that presented by Guo and El-Genk (1991). They studied the transient quenching

response of a copper surface for various orientations from vertical to a face-down position. They did not look at the horizontal (face-up) orientation. Their fully developed, high heat flux, nucleate boiling region showed a similar independence to orientation of the surface as that of Nishikawa. However, the CHF did decrease as the heater surface was rotated from vertical to increasing face-down positions. Guo and El-Genk's results at CHF compare reasonably well to Wang and Dhir's 90° results, 0.85 MW/m^2 at a superheat of 35°C and 0.61 MW/m^2 at a superheat of 20°C, respectively. While the dependence of CHF on surface orientation does require further study, we will assume for the moment that it is not the dominate effect.

The key in the development of a dry patch model in the second transition region is the solution of the transient two-dimensional conduction problem in an idealized heater (see Fig. 3a) under various boundary conditions. The wetted portion of the heater, denoted as the two-phase macrolayer region, includes the macrolayer with numerous vapor stems. Heat transfer from this region is represented by a surface-averaged, time-dependent, heat- transfer coefficient, h_2. The difficult part of the model is a realistic representation of the "dry" portion of the surface. Remember, this portion is really only dry for some fraction of the lifetime of the vapor bubble, not the entire time. A realistic estimate of both when during the vapor mushrooms lifetime the dry patch appears and how it grows must be made. During the time period in which the dry patch is formed, the heat transfer in the dry portion of the heater is represented by a surface-averaged, time-dependent, heat-transfer coefficient, h_1. The previous study of Unal et al. (1991) indicated that the initial macrolayer thickness in the dry area of the heater was extremely small so that dry patches formed almost instantaneously. In this paper, we assumed that the dry patch formation time, and consequently h_1, are zero. This provides an upper bound on the predicted contact temperature and correspondingly a lower bound on

the size of the dry patch. The determination of h_2 will be discussed in greater detail below.

For the dry patch model shown in Fig. 3a, the two-dimensional heat conduction equation in cylindrical coordinates is given for the heater by

$$\rho_h c_h \frac{\partial T}{\partial t} = k_h \left(\frac{\partial^2 T}{\partial r^2} + \frac{1}{r} \frac{\partial T}{\partial r} + \frac{\partial^2 T}{\partial z^2} \right) + Q_o \ . \tag{1}$$

The boundary conditions for the model shown in Fig. 3a are

$$\frac{\partial T}{\partial r} = 0 \quad \text{at } r = 0 \text{ and } r = r_h \tag{2}$$

$$-k_h \frac{\partial T}{\partial z} \Big|_{z=0} = q_{CHF} \quad \text{at } z = 0 \text{ for all } r \tag{3}$$

$$-k_h \frac{\partial T}{\partial z} \Big|_{z=H} = \langle h_1 \rangle \left[T(H,r,t) - T_{sat} \right] \text{ and } 0 < r < rd \ , \tag{4}$$

where

$$\langle h_1 \rangle = 0 \tag{5}$$

and $$-k_h \frac{\partial T}{\partial z} \Big|_{z=H} = \langle h_2 \rangle \left[T(H,r,t) - T_{sat} \right] \text{ for } rd < r < rs$$

$$\text{and } 0 < t < \tau \ . \tag{6}$$

Note that while the spatial averaging brackets, < >, are shown in Eqs. (4)-6), they will be dropped for convenience in the remainder of the paper.

After the vapor mushroom departs, we assume that fresh saturated liquid wets the surface. The surface temperatures in both dry patch and macrolayer regions at the time of rewet are calculated through the instantaneous contact temperature relationship (Unal et al. 1991).

To calculate an initial temperature distribution that would represent a heater before the appearance of a dry spot, no dry region was assumed. Thus, h_2 was assigned to the whole upper surface of the heater and some initial temperature distribution was estimated. The governing equation for the heater was solved numerically until convergence between two consecutive hovering periods was obtained. This calculated heater temperature distribution (found to be a function of z only) at the end of this converged hovering period was used as the "initial temperature condition" within the heater for the general problem formulation of the heat-transfer characteristics in the second transition region.

The governing equations were solved using an explicit finite-difference scheme. With small time steps, the explicit finite-difference solution yields accurate results. The experimental wall heat flux was used as the lower ($z = 0$) boundary condition and the size of the dry patch was input into the model. The size of the dry patch was varied until the predicted STA wall heat flux agreed with that input at the lower boundary.

Calculation of surface-averaged, time-dependent, heat-transfer coefficient, h_2, representing the macrolayer region (wetted region) is discussed below. The two-phase macrolayer region, shown in Fig. 3a, is characterized by numerous vapor stems in the liquid layer. Figure 3b shows the modeled geometry of only a single stem (vapor stem and the corresponding heater area that feeds the stem). As shown in Fig. 3a, the second transition region is characterized by a dry patch and a two-phase macrolayer region. Clearly, the heat transfer in the macrolayer region is far more efficient as compared with the dry region; therefore, the STA wall superheat

in the macrolayer region will be lower than the experimentally measured wall superheat, which is actually a value obtained by averaging over the entire heater surface. At CHF, the STA wall superheat for the macrolayer region can be estimated by linearly extrapolating the nucleate boiling curve of the vapor mushroom region (lower heat flux) to the second transition region, as shown in Fig. 1 (points A_{90} and A_{12}). At points A_{90} and A_{12}, the STA wall superheats are 20°C and 30°C, respectively. The measured STA wall superheats, which are really those at CHF, are 43.6°C and 121.6°C for water and the water-nickel/salt solutions, respectively. The overall heat transfer in the wetted region is represented by a time-dependent, surface-averaged, heat-transfer coefficient, h_2, which is used in the proposed model. This coefficient can be obtained from the model developed by Pasamehmetoglu et al. (1991) at points A_{90} and A_{12} of Fig. 1.

To obtain h_2, a stem calculation was performed for a copper heater representing Gaertner's heater. Calculations have shown that a 10-mm thickness can be used to represent an infinitely thick copper block.

CONSTITUTIVE RELATIONS

The single-stem calculation requires specification of the stem radius, r_s, the heater radius, r_h, corresponding to the single stem of radius, r_s, the initial macrolayer thickness, δ, as well as the triple point coefficient, m_e. The first three parameters are specified using constitutive relations, and the fourth parameter, m_e, is obtained by trial and error in such a way that the calculated value of the surface-averaged temperature matched the experimental value.

The average vapor stem radius can be calculated from

$$\frac{A_v}{A_w} = \pi r_s^2 \frac{N}{A_w} \quad , \tag{7}$$

where A_v/A_w is the heater surface void ratio and N/A_w is the number density of active sites.

The heater radius can be obtained from the geometrical relation

$$r_h = \sqrt{\frac{r_s^2}{\frac{A_v}{A_w}}} \quad . \tag{8}$$

In our previous analysis, we used Gaertner's number density relation,

$$\frac{N}{A_w} = \left(\frac{q}{!17.1}\right)^{1.5} \quad . \tag{9}$$

This equation is plotted in Fig. 4 with the symbol of open circles. However, Eq. (9) was obtained using a data set that included heat flux values only up to about 0.19 MW/m^2. So strictly speaking, Eq. (9) cannot be used for heat fluxes higher than 0.19 MW/m^2. The measured CHF is 1.554 MW/m^2. Lacking further data in our previous work, we extrapolated Eq. (9) to calculate the number density at CHF. The contact angle measurements of Wang and Dhir indicate that clean water on copper surface has a contact angle of 90°. By comparing their measured number density data for lower contact angles with Gaertner's data, they suggested that Gaertner and Westwater's water-nickel/salt solution should have a contact angle less than 18°.

In Fig. 4, we also plot the experimental number density of active sites of water-nickel/salt solution (dark circles). We can see that the extrapolated number density of clean water (contact angle of 90°) becomes less than that of water-nickel/salt solution (contact angle < 18°) at high heat fluxes. Wang's and Dhir's (1991) experimental results also indicate clearly that the number density of active

sites decreases with decreasing contact angle at a given heat flux. Also, at a given contact angle, they found that the number density varies as $q^{2.0}$. The number density relation, Eq. (9), given by Gaertner (1965) does not follow this trend. Gaertner and Westwater (1960) obtained a q exponent of 2.1. Gaertner (1965) also cites a q exponent of 1.9 obtained by Kurihara (1956). The majority of results thus point to an exponent of 2.0 as a more realistic value. Therefore, we recorrelated the number density data of Gaertner with a q exponent of 2.0. By extrapolating Wang's and Dhir's data, we determined that Gaertner's water-nickel/salt solution must have had a contact angle of 12°. Thus, in this paper, we assumed that Gaertner's water and water-nickel/salt data have contact angles of 90° and 12°, respectively. Recorrelation of Gaertner's data with a q exponent of 2.0 yields active site density values of 581.2 sites/cm^2 for water at CHF (1.554 MW/m^2) and 332.9 sites/cm^2 for the water-salt solution at CHF (1.688 MW/m^2). Dhir's water data for a contact angle of 90° give an active site density at CHF (0.61 MW/m^2) of 790.4 sites/cm^2.

In our previous study (Unal et al. 1991), we used the heater surface void ratio correlation suggested by Pasamehmetoglu and Nelson (1987), and calculated the stem diameter from Eq. (7). However, this correlation was obtained using Bhat's liquid macrolayer data and inherently assumes that the Helmholtz hydrodynamic instability criterion controls the macrolayer thickness. That analysis (Unal et al. 1991) suggests that the Helmholtz instability criterion cannot predict the formation of thin macrolayers in the dry patch region of the heater. Even when local heat fluxes were used (Chappidi et al. 1991a), the calculated values of the initial liquid macrolayer thickness were still relatively thick. This leads us to believe that the Helmholtz instability criterion is not the only mechanism controlling the macrolayer thickness and should not be used if the macrolayer thickness can be estimated from other experimental data. Here, we will use Gaertner's results.

Gaertner (1965) indicated that at a heat flux of 0.95 MW/m^2 (300000 Btu/h-ft^2), the average diameter of the stems under the vapor mushroom was 0.2007 mm and the macrolayer thickness was 0.1247 mm. He also proposed that

$$D_s = K\, q^{-0.5} \tag{10}$$

and

$$\frac{\delta}{D_s} = 0.6 \ . \tag{11}$$

The value of K in Eq. (10) for water and the water-nickel/salt solution were found using the observed stem diameters (0.2006 mm for water and 0.2438 mm for water-salt/nickel) at a heat flux of 0.95 MW/m^2 (300,000 Btu/h-ft^2) (highest heat flux at which experimental stem diameter is available). This gives K = 0.1955 for water and 0.2474 for the water-nickel/salt solution. Substituting these values together with corresponding CHF values, in Eq. (10), we obtain stem diameter values of 0.1566 mm for water and 0.1826 mm for the water-nickel/salt solution. Substituting values of stem diameter and the site density in Eq. (7), we obtain A_V/A_W values at CHF of 0.1322 for water and 0.0947 for the water-salt/nickel solution.

Wang and Dhir did not report measurements of stem diameter. To carry out our calculations for their data, we have chosen to assume that Gaertner's relations [Eqs. (10) and (11)] are applicable to their data as well. Admittedly, this assumption is subject to debate and will be discussed further in Sec. V. However, we are attempting here only to verify the hypothesis of hot-spot-controlled CHF; from this viewpoint, we believe that even an approximation such as this will nevertheless

help us to reach useful conclusions. Similar calculations as in the previous paragraph yield an A_v/A_w value of 0.3403 for a contact angle of 90°.

The data used in the single-stem calculations for the various runs are summarized in Table I. The surface-averaged, time-dependent, heat-transfer coefficient h_2, which represents the transient heat transfer in the macrolayer region, was calculated by dividing the calculated instantaneous surface-averaged wall heat flux with the calculated instantaneous surface-averaged wall superheats. Figure 5 shows the calculated transient heat- transfer coefficients for Gaertner's water and water-nickel/salt data at two different heat flux levels. In each case, the triple-point evaporation coefficient listed in the inset in Fig. 5 was obtained to match the experimentally measured surface-averaged wall temperature. The triple-point coefficient decreases with increasing heat flux. This is perhaps related to the decrease in the average stem diameter.

The heat-transfer coefficient, h_2, shown in Fig. 5, is relatively high at the beginning of the new hovering period. This is because when fresh saturated liquid wets the surface, the surface contact temperature decreases. Conduction within the heater then transports significant energy early in the mushroom's lifetime to reheat the surface. Later in the time window from 0.05τ to τ, h_2 gradually increases. In these calculations, the evaporation at the triple point is the dominant mechanism (Unal et al. 1991). For a given contact angle, the heat transfer coefficient decreases with as the heat flux decreases. Also, for a given heat flux, it decreases as the contact angle decreases. This is consistent with Wang's and Dhir's experimental observations; the boiling curve is shifted to the right with decreasing contact angle, so that at the same heat flux the wall temperature is high for low contact angles. We will discuss the calculated values of the heat-transfer coefficients for Wang's and Dhir's data later at the end of Sec. III.

III. RESULTS AND DISCUSSION

In this section, we will first discuss the estimation of liquid-solid contact temperature at the onset of CHF in Gaertner's experiments and then compare the estimates with available data. Second, we will examine whether these temperatures are attainable in the tests of Wang and Dhir.

In all calculations, the dry patch is assumed to occur instantaneously, that is, the complete dry patch is formed at t = 0. As noted earlier, this a bounding calculation that yields the maximum possible contact temperature. We will first discuss the results of applying the model to Gaertner's data. Gaertner's STA heat flux and superheat at CHF for clean water (contact angle estimated here to be 90°) were 1.554 MW/m^2 and 43.6°C, respectively. For these conditions, our calculations show that the dry patch radius required is 15.2 mm. The local instantaneous temperature at the end of the converged hovering period at the center of the dry patch, T_{TL}, was 179.7°C. This local-instantaneous temperature can be considered to be the critical liquid-solid contact temperature for CHF to occur for this bounding case—clean water, with a contact angle of 90° and a CHF of 1.554 MW/m^2. The other values calculated for this case, run 1, are listed in Table II.

The radial instantaneous wall superheat profiles for run 1 at six axial elevations are shown in Fig. 6. The instantaneous temperatures on the boiling surface of the heater gradually decrease to typical values calculated for the macrolayer region. The variation of temperature at the bottom of the heater is relatively small.

In run 2, we repeated the calculation for Gaertner's and Westwater's water-nickel/salt data using the heat-transfer coefficient, h_2, represented in Fig. 5. The experimental STA wall superheat at CHF (1.688 MW/m^2) for this case is 121.6°C. The dry patch size required was found to be 20.6 mm. The local instantaneous temperature at the end of the converged hovering period at the center of the dry

patch, T_{TL}, was 268°C. The instantaneous radial wall temperature profiles for this run are presented in Fig. 7.

From the above results, it is clear that the liquid-solid contact temperature increases as the contact angle decreases. Figure 8 is a plot of the dimensionless liquid-solid contact temperature at the onset of CHF as a function of the contact angle. The figure also includes experimental liquid-solid contact temperature data reported by Ramilison and Lienhard (1987) at the onset of film boiling. Considering the uncertainty in the inferred contact angle, the calculated dimensionless contact temperatures agree reasonably well with the data of Ramilison and Lienhard. We can make the following inferences from this figure:

(1) The controlling mechanisms for the CHF and quenching could be similar. That is, both processes are controlled by the ability of liquid to contact the hot surface.

(2) The critical contact temperature decreases with increasing advancing contact angle. The contact angle at the onset of CHF can be characterized by the advancing contact angle just as in the case of the onset of film boiling. If CHF is the consequence of the inability of liquid to wet a previously dry area, clearly the relevant angle is the advancing contact angle.

(3) When the advancing contact angle approaches zero (perfectly wetting fluid), the upper limit of the contact temperature is the homogeneous nucleation temperature of the liquid.

Different values of CHF have been reported in the literature for pool boiling of water on copper surfaces. As we described earlier, Wang's and Dhir's tests with a 90° contact angle yielded a CHF of 0.61 MW/m^2; but Gaertner's clean water experiments,

also considered to have had a contact angle of 90°, yielded a CHF of 1.554 MW/m^2. Although there are differences in the heater geometry, both heaters have high thermal inertia and large characteristic lengths. Depending upon the surface conditions, we can expect the values of CHF to vary. However, if the hypothesis we propose for the occurrence of CHF is correct, one should expect that a local point on the heater surface should reach the critical liquid-solid contact temperature in all cases, even if the CHF values themselves are different. Below we will examine whether this condition can be satisfied for Wang's and Dhir's pool boiling data.

We will discuss the case of a 90° contact angle and will perform our analysis at a heat flux of 0.7 MW/m^2, which is little above the CHF value of 0.61 MW/m^2. In the absence of stem diameter or surface void fraction information in Wang's and Dhir's paper, we have made the following assumptions:

(1) Gaertner's relations between stem diameter and heat flux, and that between the macrolayer thickness and stem diameter are valid in this case.

(2) The triple-point evaporation coefficients tuned to predict Gaertner's data are also valid. This coefficient depends upon the shape of the vapor-liquid interface near the triple point. Currently, we do not have a mechanistic model to predict the heat transfer from this microscopic region and we assume that it is heat flux dependent for a given contact angle. If the average stem diameter is very much different in magnitude in Wang's and Dhir's tests than that reported by Gaertner, the triple-point coefficients and corresponding surface-averaged heat-transfer coefficient in the two-phase macrolayer region could be different.

(3) The rectangular geometry of the test section can be represented by a circular shape by preserving the total surface area.

At a heat flux of 0.7 MW/m^2, Gaertner's 90° data show that the STA wall superheat was 17.2°C. The triple-point coefficient for this case was found to be 1.065e-08 kg/m s°C. This is indicated in Fig. 5. If this coefficient is used in a stem calculation at the same heat flux, 0.7 MW/m^2, the surface-averaged transient heat-transfer coefficient is higher compared with values obtained for Gaertner's data at the same conditions. This can be seen in Fig. 9. This increase is due to the higher number density of active sites on Wang's and Dhir's test surface. This causes the surface void ratio to be higher, and correspondingly, the heater radius per stem (in the stem calculation) decreases significantly. The resulting STA wall superheat becomes very low, 3.4°C, in the two-phase macrolayer region. Results of this case are l ed in Tables I and II as run 3.

The calculated STA wall superheat in the two-phase macrolayer region is much less than the value of 20.6°C reported by Wang and Dhir. This indicates that some part of the heater must already be dry so that the temperature there would be well over 20.6°C. Alternatively, the lower calculated STA temperatures could be the result of assumptions 1 and 2 mentioned above. In Sec. V, we examine the sensitivity of our calculations to the various parameters. This will give a better indication of the impact of assumptions (1) and (2) on our results.

When we match the reported STA wall temperature using our two-region model shown in Fig. 3a, we find that the temperature at the center of dry patch region is 161.6°C (see Fig. 10, which shows the instantaneous radial temperature profile at four axial elevations). This value is reasonably close to the critical contact temperature of 179.7°C that we obtained based on Gaertner's data. This indicates that a local point on the heated surface could reach the critical liquid-solid contact temperature in Wang's and Dhir's tests with a 90° contact angle, causing the occurrence of CHF at lower values.

IV. SENSITIVITY ANALYSIS

As we mentioned in the preceding section, our calculation of the dry spot temperature in Wang's and Dhir's experiments was carried out by assuming that results from Gaertner's data could be applied to this case as well. Specifically, we used values of the stem diameter, D_s, and the triple-point evaporation coefficient, m_e, derived from Gaertner's data. In this section, we will examine the sensitivity of our results to changes in the values of these parameters. We will also look at the effect of changes in the nucleation site density, N/A_w, the nodalization scheme, and the heater thickness.

In our original calculation of the dry spot temperatures in Wang's and Dhir's 90° contact angle experiments, we used a value of 1.065e-8 kg/m s °C for the triple-point coefficient. When we carried out the calculations again, with a value of 3.78e-09 kg/m s °C (obtained to match Gaertner's CHF of 1.554 MW/m^2), the surface-averaged heat-transfer coefficient, h_2, was decreased. The STA wall superheat in the two-phase macrolayer region in this case was 8.2°C. The temperature at the center of the dry region was found to be 157.2°C. Results of this case are listed in Tables I and II as run 4. A three-fold decrease in the triple point coefficient causes a two-fold increase in the STA wall superheat on the wet region, but has decreased the calculated dry spot superheat by less than 7.2%. It is clear that assumption (2) has a negligible effect on our results.

As we mentioned earlier, while making the calculations for Wang's and Dhir's data, we were compelled to assume that Gaertner's vapor stem relations can be applied to this case as well. However, the validity of this assumption is clearly not established. With this in mind, we tested the sensitivity of the calculated values of the critical rewetting temperatures with respect to the vapor stem diameter. This will give a clearer picture of the impact of the assumption on our results. In run 5,

listed in Tables I and II, we changed the vapor stem diameter to 0.1 mm. Keeping the triple-point coefficient and the heater diameter per stem the same as in run 4, we found that the calculated rewetting temperature is 156.5°C. Although the vapor stem diameter was decreased by 57%, the calculated surface-averaged heat-transfer coefficient on the wet side decreased only by 15%. The surface-averaged wall superheat on the wet side decreased only by 6%. Subsequent calculations of the dry patch problem show that the critical rewetting superheat has been reduced only by 1.2%. It appears therefore that only a small error is introduced in our calculations as a result of our applying Gaertner's vapor stem relations to Wang's and Dhir's data.

In run 6, listed in Table I, we repeated the stem calculations for the case of run 4, except that we decreased the nucleation site density such that the effective heater diameter per stem increased to 0.30 mm. This in effect reduces the area void fraction by 55%. The triple-point coefficient and the vapor stem diameter were kept the same as in run 4. With these input data, the wet region surface-averaged heat-transfer coefficient reduced by over 47%. This makes it clear that the wet region heat-transfer coefficient is highly sensitive to the active site density N/A_w. The surface- and time-averaged temperature in the wet region for this stem calculation was found to be 116.5°C. This value is fairly close to the experimentally measured surface-and time-averaged value of 120.6°C. This suggests that in this case, almost the entire heated surface could be covered with the two-phase macrolayer and that the high-temperature dry spots, if any, must be relatively small in area.

Another single stem calculation was carried out keeping the parameters the same as in run 4, but changing the nodalization scheme used in the radial direction. Whereas the vapor stem radius was divided into 8 radial segments in run 4, this time we used 18 segments. The results indicate that change in the nodalization has no significant effect on the surface-averaged wet region heat-transfer coefficient and correspondingly the surface- and time-averaged wall temperature. We also

investigated the effect of the heater thermal mass on the results; to do this, we changed the thickness of the heater to 20 mm. Again, the results suggest that the heater thermal mass has no significant effect, as long the heater is one that can be regarded as an "infinitely thick" heater.

The sensitivity of the calculated heat-transfer coefficients and surface temperatures to the nucleation site density points to another condition for the occurrence of the second transition region. For the high nucleation site densities measured by Wang and Dhir, the calculated temperatures on the wet side are very low. Therefore, although the temperatures of the dry areas reach the level of the critical rewetting temperature, the surface-averaged temperatures on the entire top surface of the heater do not show appreciable increases. Under these conditions, the second transition region characterized by a decrease in the slope of the boiling curve will not be observed. In the earlier study (Unal et al. 1991) we had proposed that one condition for the occurrence of the second transition region is that the heater thickness must be relatively large. The present study indicates that in addition to this, the nucleation site density must be below a critical value for the occurrence of a second transition region Above this critical value, lower wall temperatures in the macrolayer region prevent the surface-averaged temperature from causing a change in the slope of the boiling curve. This also implies that measurements of STA wall temperature, which provide indications as to whether the second transition region exists, cannot be used as a litmus test to make conclusions about the existence of dry patches on the heater surface. Whether dry patches can eventually cause a second transition region to occur appears to depend strongly on the active nucleation site density.

The obvious question is why do experimental studies not report seeing such cold spots? One possible reason is that the temperatures we are talking about here are local, instantaneous values. Whether these variations can be detected in

experiments would depend to a large extent on the location of the thermocouples relative to the dry patches. As discussed earlier, currently we assume that there is only a single dry patch circular in shape on the surface; site activation and dry patch growth are not considered. Furthermore, we also assume two-dimensional geometry. In reality, the dry patches are numerous and spatially distributed on the heater surface. These assumptions are idealizations of what is in reality a very complex phenomenon. More accurate modeling of such a variation requires a three-dimensional approach. If such a model is used to predict the critical liquid-solid contact temperatures, the values we report here for the liquid-solid contact temperature could also be different. The three-dimensional modeling will be considered in a future publication.

VI. SUMMARY AND CONCLUSIONS

The current model employed to study the boiling phenomenon in the second transition region of saturated pool nucleate boiling on a horizontal surface is a two-dimensional transient-conduction model representing the heater and its boiling surface. The wetted portion of the heater, denoted as having a time-dependent surface-averaged heat-transfer coefficient h_2, characterizes a macrolayer having numerous vapor stems. The heat- transfer coefficient h_2 was obtained from the model developed by Pasamehmetoglu et al. (1991).

The constitutive relations in determining the stem radius, heater radius and the surface void ratio for Gaertner's clean water and water-nickel/salt solution were reevaluated in the light of new results from Wang and Dhir (1991). In analyzing the Wang and Dhir data, the stem diameter expression obtained from Gaertner's tests was used. This resulted in relatively high surface void ratios because of the significantly higher number densities of active sites. Based upon the conclusions reached in the previous study of Unal et al. (1991), we assumed that a stationary dry

patch circular in shape occurs instantaneously in the dry patch region. Therefore, the bounding case of no heat transfer in the dry portion of the heater is considered.

The main conclusions of the present study are as follows:

(1) The liquid-solid contact temperature at the center of the dry patches at the onset of CHF was found to vary between 268°C and 179°C for the data of Gaertner (1965) for contact angles ranging from 12° to 90°. These temperatures were in reasonable agreement with the liquid-solid contact temperatures at the onset of ... boiling reported by Ramilison and Lienhard (1987). This supports the hypothesis that the controlling mechanisms for CHF and quenching could be similar. The occurrence of dry patches on the heated surface themselves is not sufficient to cause CHF. The temperature at the center of the dry patch must first reach a critical value above which liquid-solid contact is no longer possible.

(2) Calculations based on the data of Wang and Dhir (1991) showed that the surface temperatures on the wet regions are very low. This suggests that dry patches must exist on their heater, so that the surface-averaged temperatures would be as measured in their experiments.

(3) We have further examined the reasons why the second transition region characterized by a decrease in the slope of the boiling curve has not been observed in all experiments. In addition to the requirement presented in Unal et al. (1991) that the heater thickness must be large, an additional criterion determined here is that the active nucleation site density must be below a critical value. Additional experimental efforts are necessary to fix the value of this critical site density.

The results obtained from this analytical study are presented in the hope of aiding additional understanding of the mechanism governing CHF. Experiments could be devised to investigate the dry patch characteristics further. Closer attention needs to be paid to the measurement of spatial variations in surface temperatures.

VI. REFERENCES

Borishansky, V. M., 1965, "An Equation Generalizing Experimental Data on the Cessation of Bubble Boiling in Large Volume of Liquid," *Zh. Tekh. Fiz.* **26**(7),452-456.

Chang, Y. P., 1957, "A Theoretical Analysis of Heat Transfer in Natural Convection and in Boiling", Paper 56-A42, ASME, New York, 1956. *Trans. ASME.* **79,** 1501-1513 .

Chang, Y. P., and Snyder, N. W., 1960, "Heat Transfer in Saturated Boiling," *Chem. Engr. Prog. Symp. Ser.* **56**, 30, 25-38.

Chappidi, P, Unal, C., Pasamehmetoglu, K. and Nelson, R.A., 1991b, "On the Relation Between the Macrolayer Thickness and the Vapor-Stem Diameter in the High-Heat-Flux, Pool Nucleate Boiling Region," *Int. Communications in Heat & Mass* Transfer **18**, 2, pp.195-205, March-April 1991.

Chappidi, P., Unal, C., Pasamehmetoglu, K. and Nelson, R.A., 1991a, "Saturated Pool Boiling Mechanisms at High Heat Fluxes: A Superposition Method for Averaging the Local-Instantaneous Variation in Wall Temperatures and Heat Flux With a Statistical Distribution of Active Cavities," HTD-Vol. 159, pp. 119-

130, 28th National Heat Transfer Conference, Minneapolis, MN (1991), Los Alamos National Laboratory document LA-UR-90-4385 (1990).

Gaertner, R. F., 1965 , "Photographic Study of Nucleate Pool Boiling on a Horizontal Surface," *Journal of Heat Transfer* **15**, 401-428.

Gaertner, R. F., and Westwater, J. W., 1960, "Population of Active Sites in Nucleate Boiling Heat Transfer," *Chem. Engng. Prog. Symp. Ser.*, **56**, (30), 39-48.

Guo, Z., and El-Genk, M. S., 1960, "An Experimental Study of the Effect of Surface Orientation on Boiling Heat Transfer During Quenching," ASME paper 91-WA-HT-1, ASME Winter Annual Meeting, Atlanta, Georgia, December 1991.

Haramura, Y. and Katto, Y., 1983, "A New Hydrodynamic Model of Critical Heat Flux, Applicable Widely to Both Poll and Forced Convection Boiling on Submerged Bodies in Saturated Liquids," *Int. J. Heat Mass Transfer* **26** (3), 389-399.

Hesse, G., 1973, "Heat Transfer in Nucleate Boiling, Maximum Heat Flux and Transition Boiling," *Int. J. Heat Mass Transfer* **16**, 1611-1627.

Hsu, Y. Y. and Graham, R. W., 1976, Transport Processes in Boiling and Two-Phase Systems, McGraw-Hill Book Company.

Kirby, D. B. and Westwater, J. W., 1965, "Bubble and Vapor Behavior on a Heated Horizontal Plate During Pool boiling Near burnout," *Chem. Eng. Progr. Symp. Ser.* **61**, (57).

Kurihara, H.M., 1956, Ph.D. thesis, Purdue University, Lafayette, Indiana.

Kutateladze, S. S., 1956, "A Hydrodynamic Theory of Changes in Boiling Process Under Free Convection," *Izu. Akademia Nouk Otdelarie Tekh. F12* **26** (7), 452-456.

Liaw, S.P. and Dhir, V.K., 1989, "Void Fraction Measurements During Saturated Pool Boiling of water on Partially wetted Vertical Surfaces," *J. of Heat Transfer* **111**, 731-738.

Liaw, S.P., 1988, "Experimental and Analytical Study of Nucleate and Transition Boiling on Vertical Surfaces," Ph.D. Dissertation, Mechanical Engineering Department, University of California, Los Angeles.

Lienhard, J.H., 1982, "Corresponding States Correlations for the Spinodal and Homogeneous Nucleation Temperature," *ASME J. of Heat Transfer* **104**, (23), 379-381.

Nishikawa, K., Fujita, Y., and Ohta, H., 1974, "Effect of Surface Configuration on Nucleate Boiling Heat Transfer," *Int. J. Heat Mass Transfer* **27**, 1559-1571.

Ouwerkerk, H.J., Van, 1972, "Burnout in Pool Boiling the Stability of Boiling Mechanism," *Int. J. Mass Heat Transfer* **15**, 25-34 .

Pasamehmetoglu, K., Chappidi, P.R., Unal, C. Nelson, R.A., 1991 "Saturated Pool Boiling Nucleate Boiling Mechanisms at High Heat Fluxes," submitted to *Int. J. of Heat Mass Transfer*.

Ramilison, J.M. and Lienhard, J.H., 1987, "Transition Boiling Heat Transfer and Film Transition Regime," *J. of Heat Transfer* **109**, 746-752.

Rohsenow, W. and Griffith, P., 1956, "Correlation of Maximum Heat Flux Data for Boiling of Saturated Liquid," *Chem. Engr. Symp. Ser.* **52**, 18.

Sterman, L. S., 1953, "Theory of Heat Transfers in Boiling Liquids," *Zh. Tekh. Fiz.* **23**, (2), 341-351.

Unal, C., Vincent, D., and Nelson, A. R., 1991, "Unifying the Controlling Mechanisms for the Critical Heat Flux and Quenching: The Ability of Liquid to Contact the Hot Surface," HTD-Vol. 159, pp. 130-140, 28th National Heat Transfer Conference, Minneapolis, MN (1991), Los Alamos National Laboratory document LA-UR-91-933.

Wang, C.H., and Dhir, V.K., 1991, "Effect of Surface Wettability on Active Nucleation Site Density During Pool Boiling of Water on a Vertical Surface," HTD-Vol. 159, pp 89-96, 28th National Heat Transfer Conference, Minneapolis, MN (1991).

Yu, C. L., and Mesler, R. B., 1977, "Study of Nucleate Boiling Near the Peak Heat Flux Through Measurements of Transient Surface Temperature," *Int. Journal of Heat Mass Transfer* **20**, 827-840.

Zuber, N. 1959, "Hydrodynamic Aspects of Boiling Heat Transfer," Ph.D. Thesis, University of California, Los Angeles, CA.

Zuber, N., 1958, "Stability of Boiling Heat Transfer," *Trans. ASME* **80** 711-720.

Zuber, N., Tribus, M., and Westwater, J. W., 1961, "The Hydrodynamic Crisis in pool Boiling of Saturated and Subcooled Liquids," 2nd Int. Heat Trans. Conf. paper 27, Denver, CO.

TABLE I. DATA USED SINGLE STEM CALCULATION FOR VARIOUS RUNS

Run	q (MW/ m^2)	θ	m_e (kg m-s °C)	N/A_w (#/ cm^2)	A_v/A_w	r_s (mm)	r_h (mm)	δ (mm)	ΔT_{av} on wet side (calculated)	ΔT_{av} top expt
1	1.554	90°	3.780×10^{-9}	581.2	0.1322	0.0783	0.2153	0.0978	20.01 °C	43.6°
2	1.688	12°	5.300×10^{-9}	332.9	0.0947	0.0913	0.2967	0.1141	29.22 °C	121.6°
3	0.700	90°	1.065×10^{-8}	790.4	0.3403	0.1167	0.2000	0.1458	3.37 °C	20.6°
4	0.700	90°	3.780×10^{-9}	790.4	0.3403	0.1167	0.2000	0.1458	8.16 °C	20.6°
5	0.700	90°	3.780×10^{-9}	790.4	0.0625	0.0500	0.2000	0.0937	8.67 °C	20.6°
6	0.700	90°	3.780×10^{-9}	353.7	0.1509	0.1167	0.3000	0.1458	16.52 °C	20.6°
7	0.700	90°	1.065×10^{-8}	117.7	0.1322	0.1167	0.4959	0.1458	17.23 °C	17.7°

TABLE II. RESULTS OF DRY PATCH MODEL

Run	q (MW/m^2)	θ (deg)	r_d (mm)	r_d/r_h	ΔT_{av} (°C)	ΔT_{BL} (°C)	ΔT_{BR} (°C)	ΔT_{TL} (°C)	ΔT_{TR} (°C)
1	1.554	90	15.2	0.60	43.6	99.8	76.3	79.7	28.6
2	1.688	12	20.6	0.81	122.4	189.1	152.9	167.9	80.9
3	0.700	90	24.8	0.54	20.7	65.8	29.3	57.2	9.8
4	0.700	90	27.3	0.60	20.6	70.3	25.1	61.6	4.5
5	0.700	90	24.2	0.53	20.8	65.2	29.6	56.5	10.2

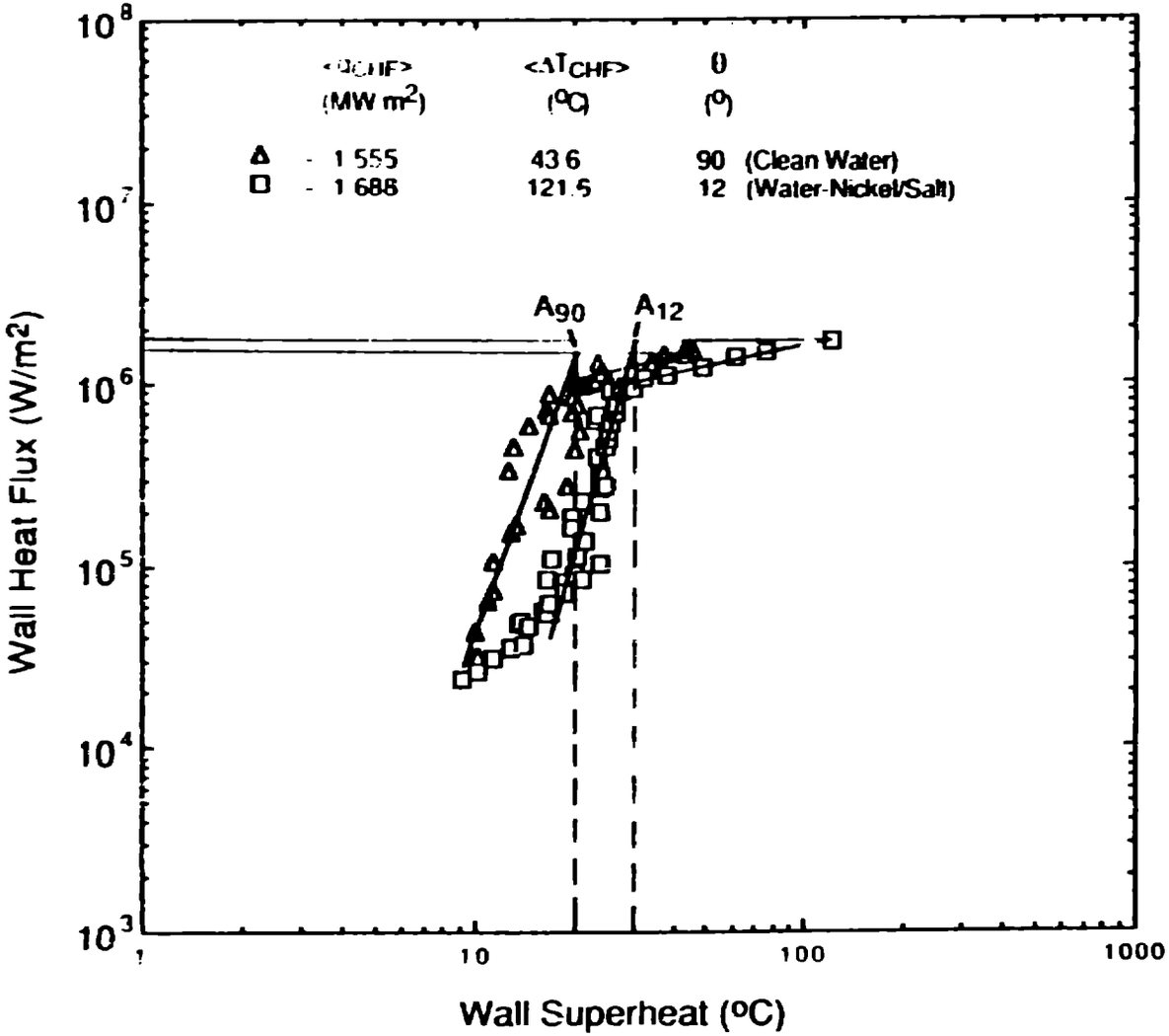

Fig. 1. The pool boiling data of water and water-nickel/salt solution on horizontal copper cylinders reported by Gaertner (1963) and Gaertner and Westwater (1960).

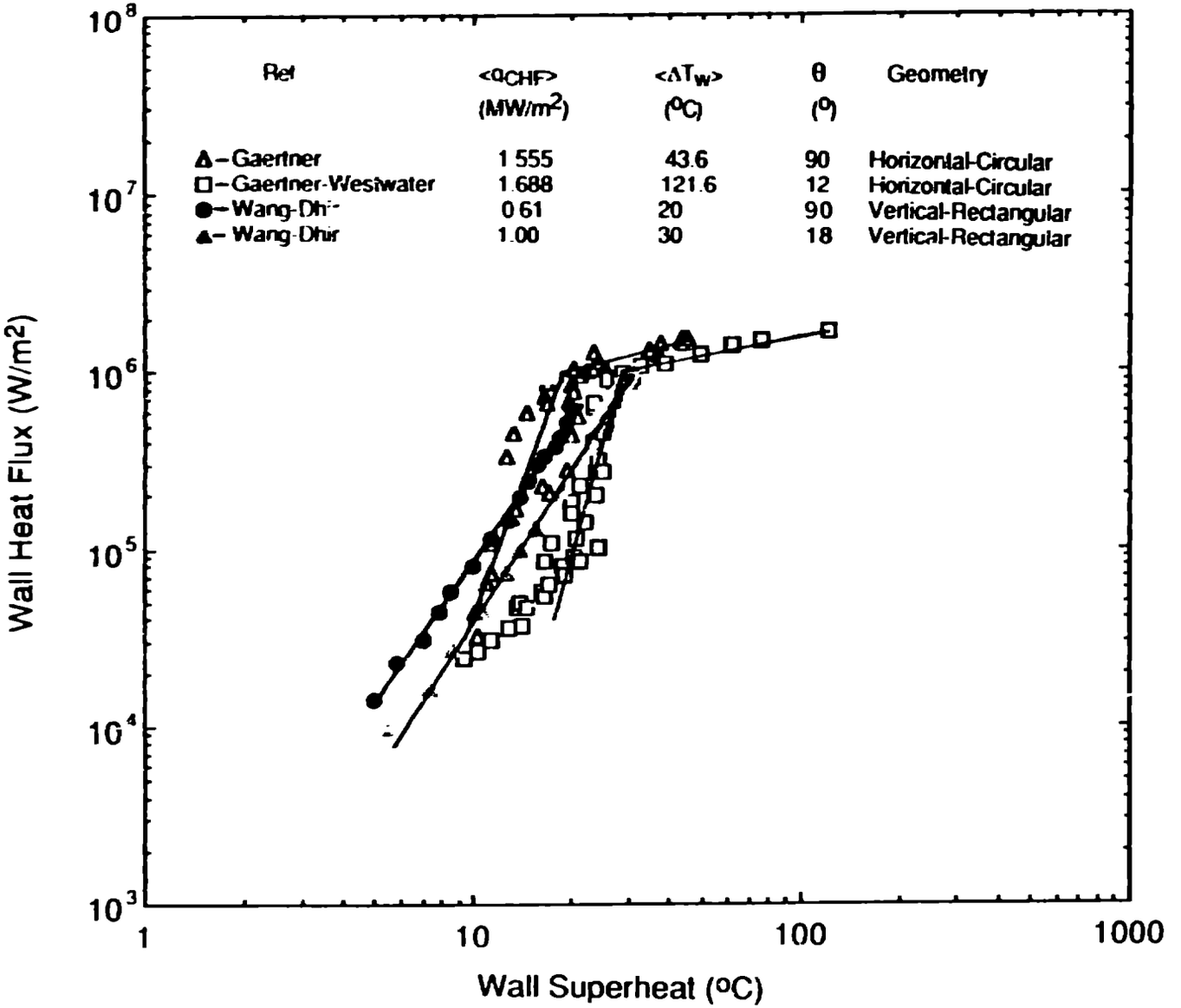

Fig. 2. Pool boiling data of water on copper heaters for different contact angles.

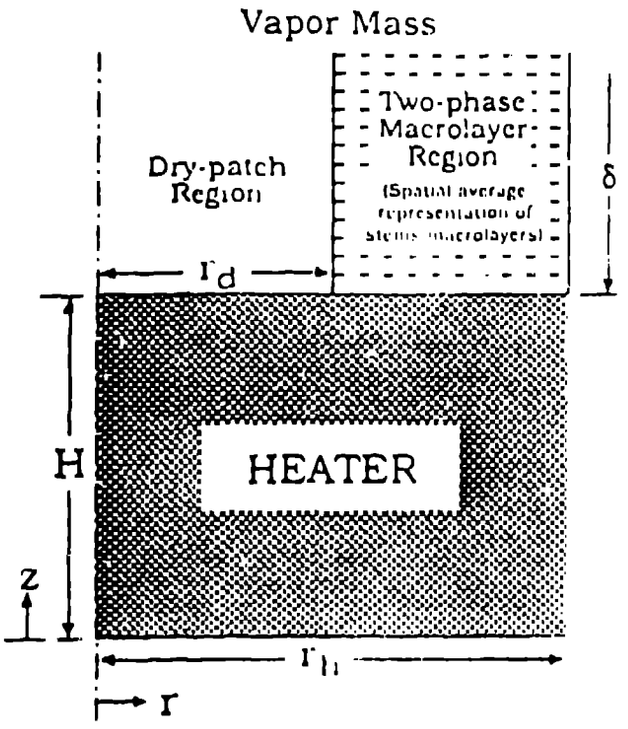

Fig. 3a. Sketch of the proposed heat-transfer model for the second transition region of the nucleate boiling.

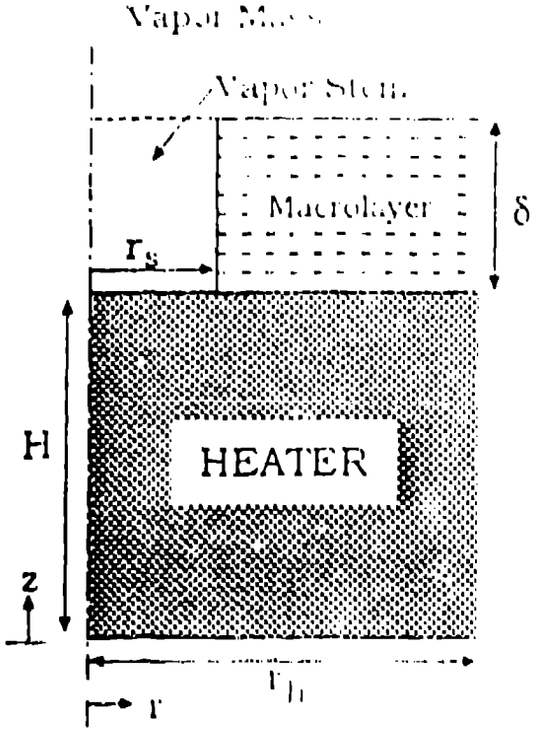

Fig. 3b. Sketch of heat-transfer model (stem model) for pool boiling at high heat fluxes developed by Pasamehmetoglu et. al. (1991).

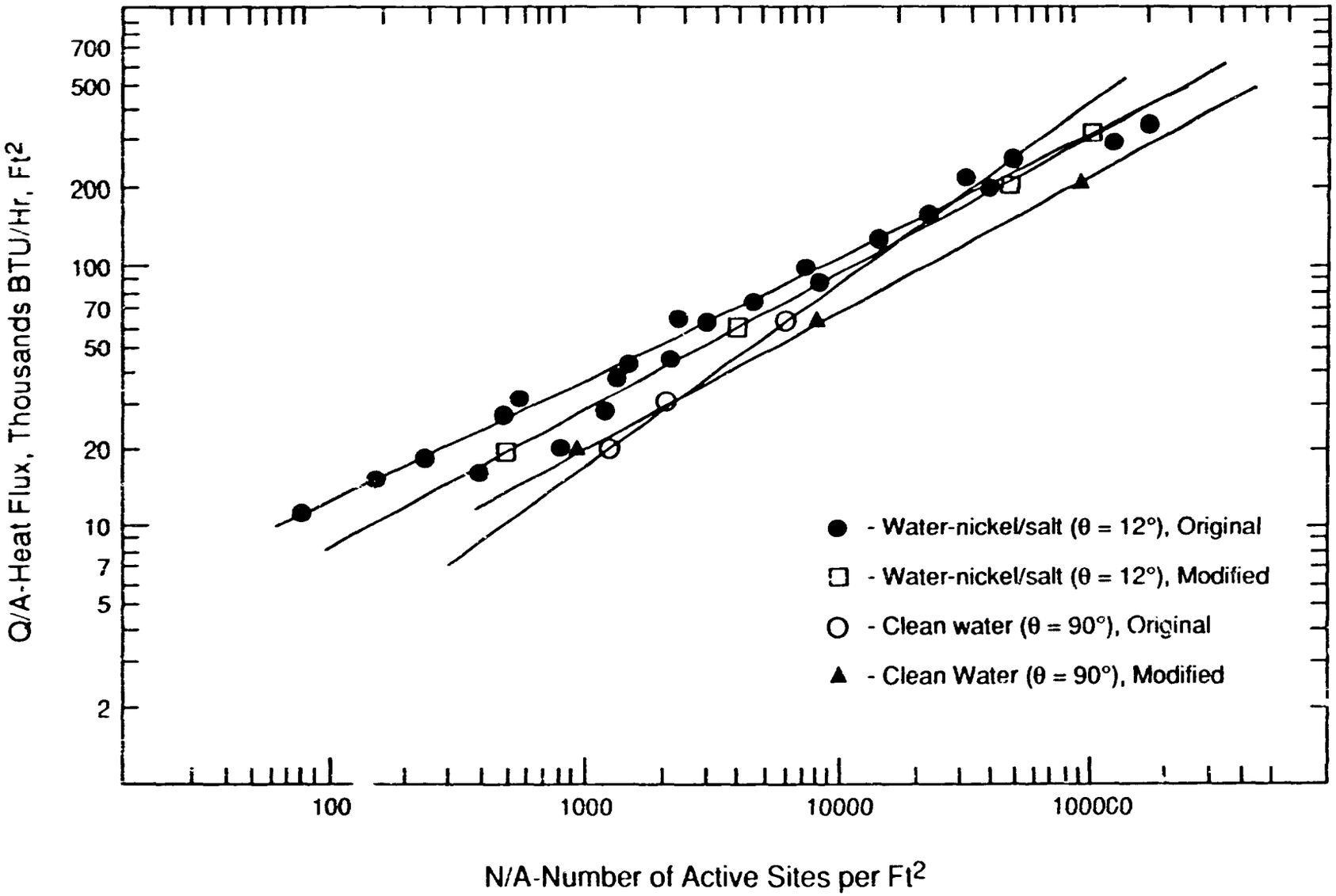

Fig. 4. The number density of active sites as a function heat flux for Gaertner's water and water-nickel/salt solution data.

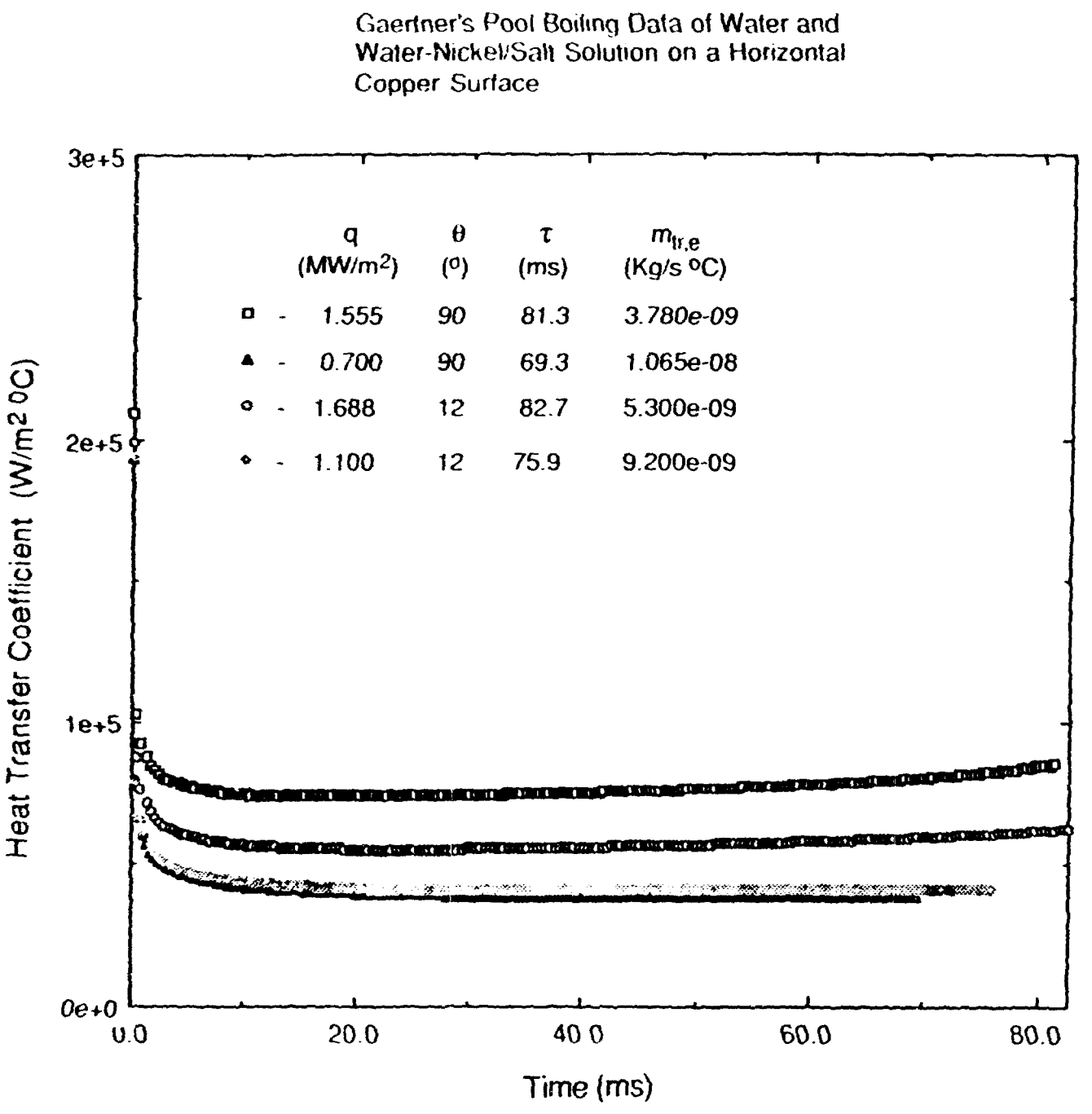

Fig. 5. *The* surface-averaged transient heat-transfer coefficient in the two-phase macrolayer region of the heater for different heat fluxes and contact angles.

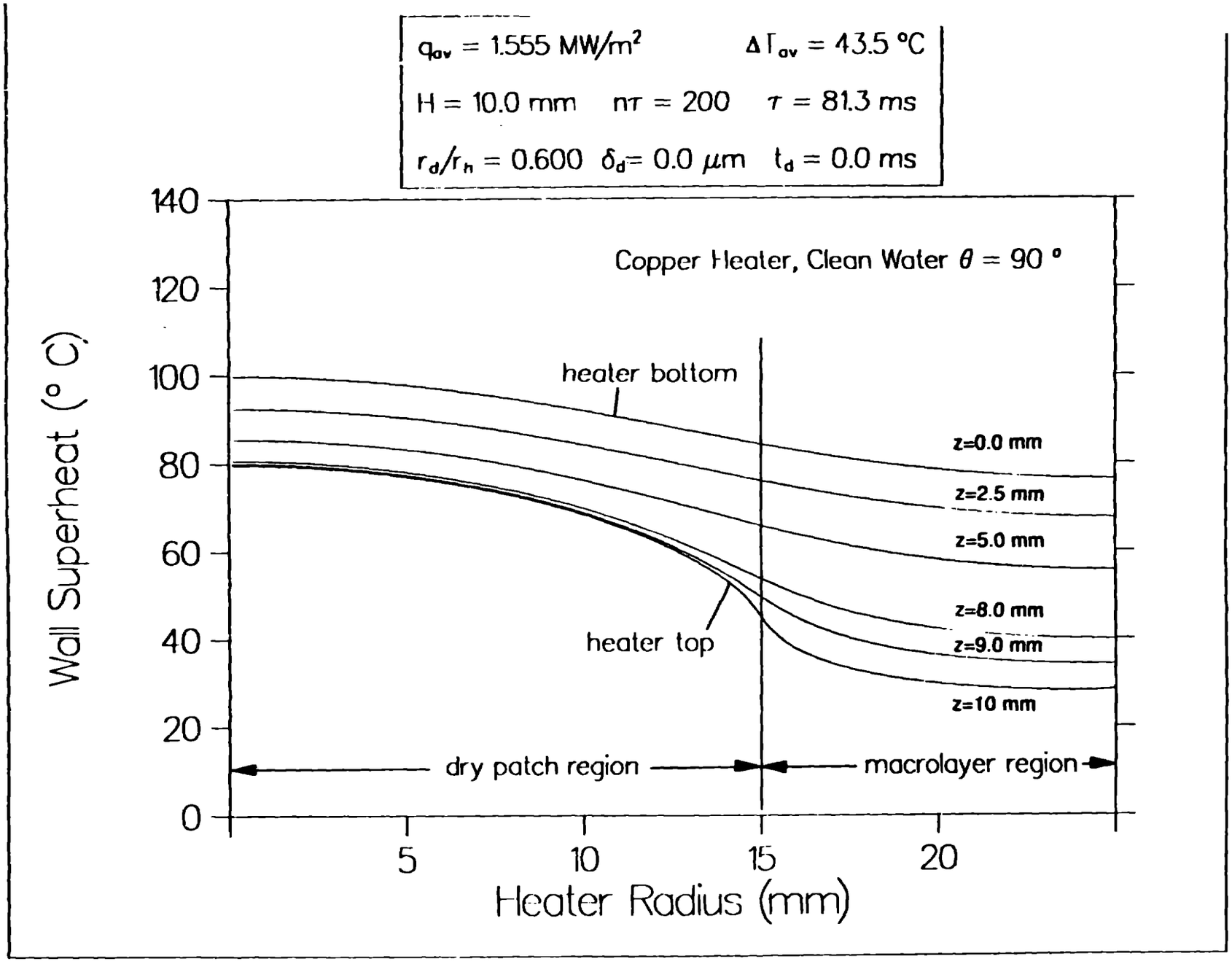

Fig. 6. The instantaneous radial wall temperature profiles at six different elevations at the end of converged hovering period for a CHF of 1.55 MW/m² and a 90° contact angle.

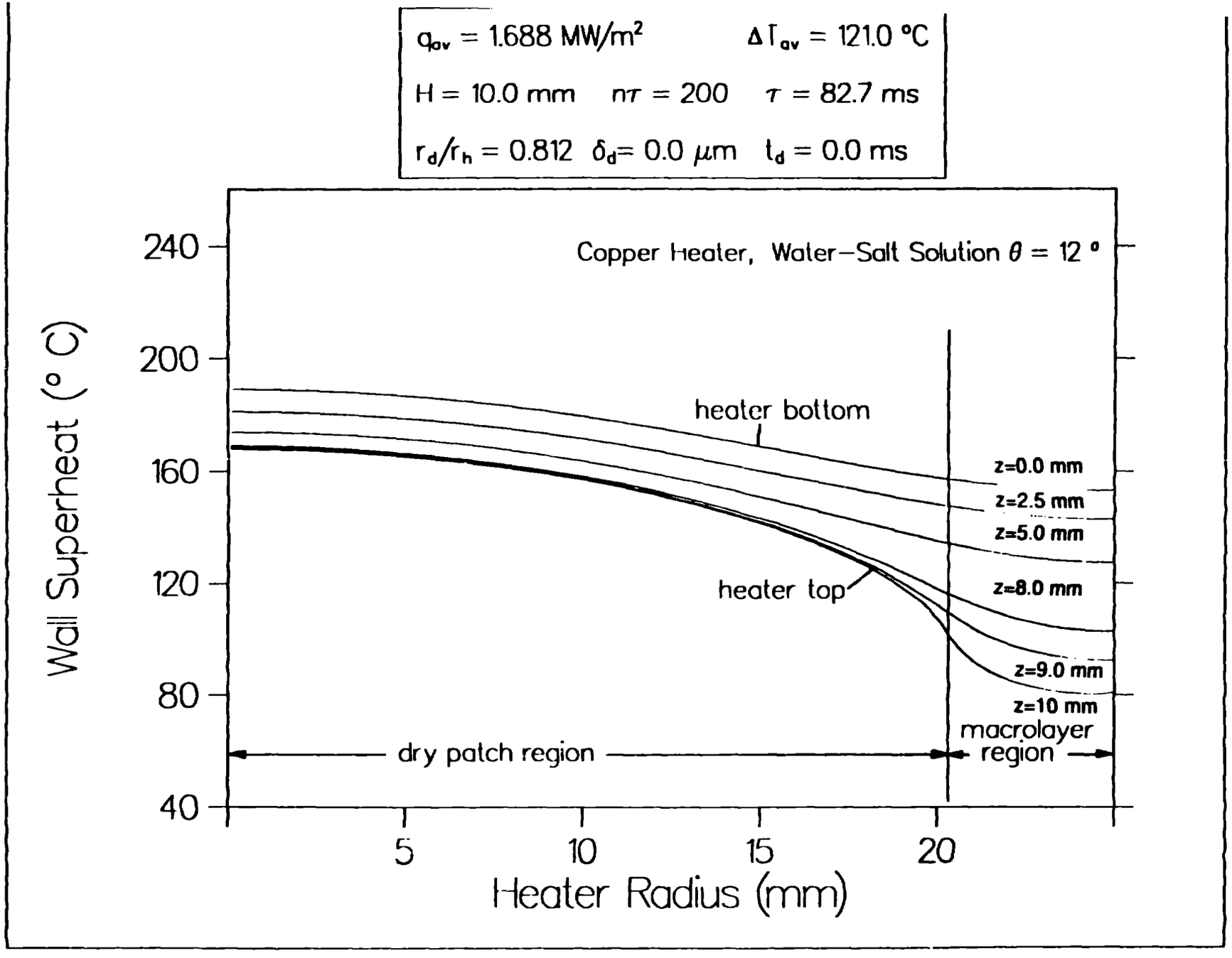

Fig. 7. The instantaneous radial wall temperature profiles at six different elevations at the end of converged hovering period for a CHF of 1.688 MW/m^2 and a 12° contact angle.

	Ref.	θ (°)	r_d/r_h	ΔT_{av} (°C)	q_{av} (MW/m^2)	T_{rew} (°C)
△	Present	90	0.60	43.6	1.55	179.7
□	Present	12	0.81	122.4	1.67	267.9
●	Ramilison and Leinhard,1987					
■	Berenson (from Ramilison and Leinhard, 1987)					

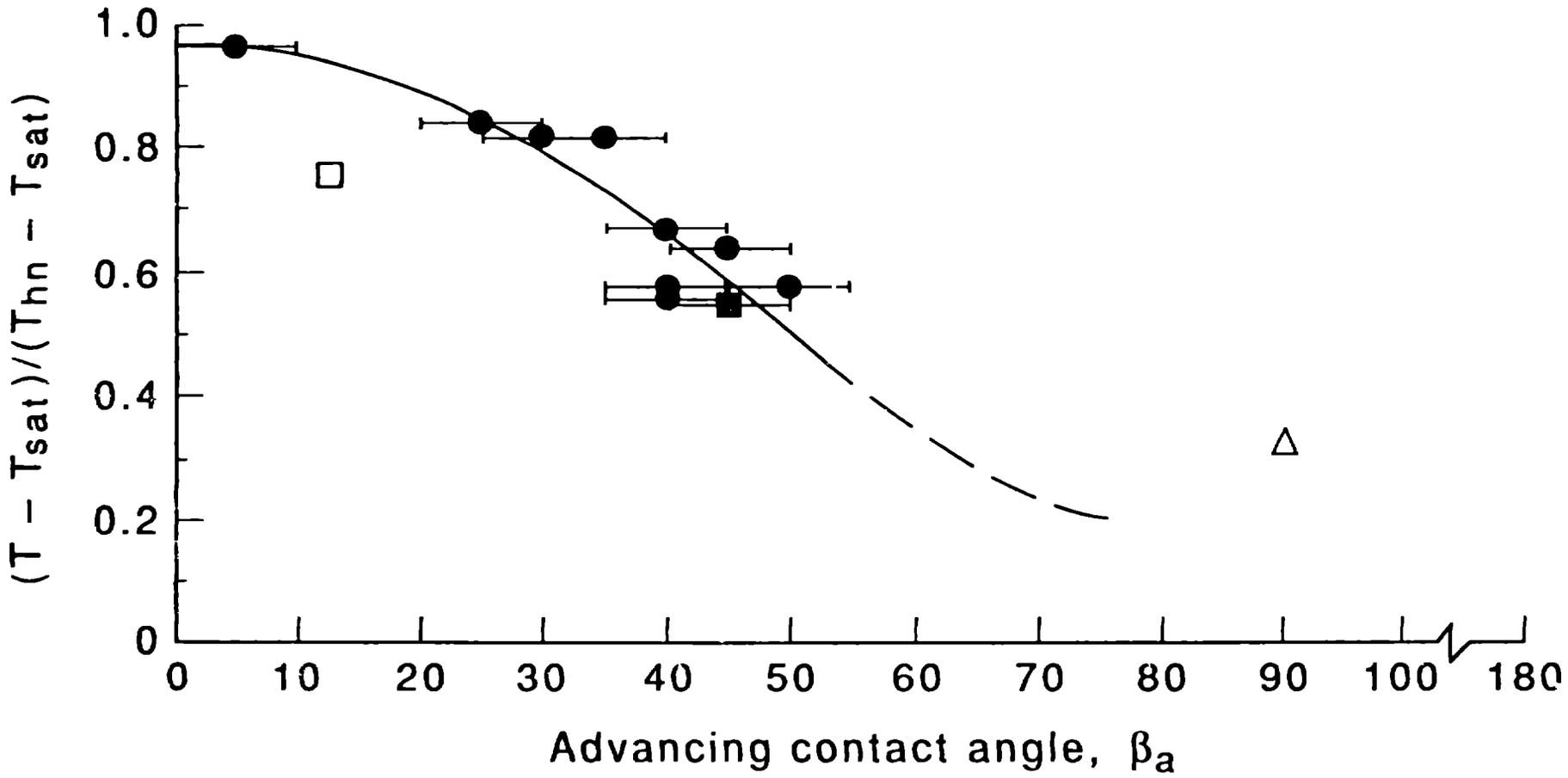

Fig. 8. The liquid-contact temperatures at the onset of CHF and film boiling as a function of contact angle.

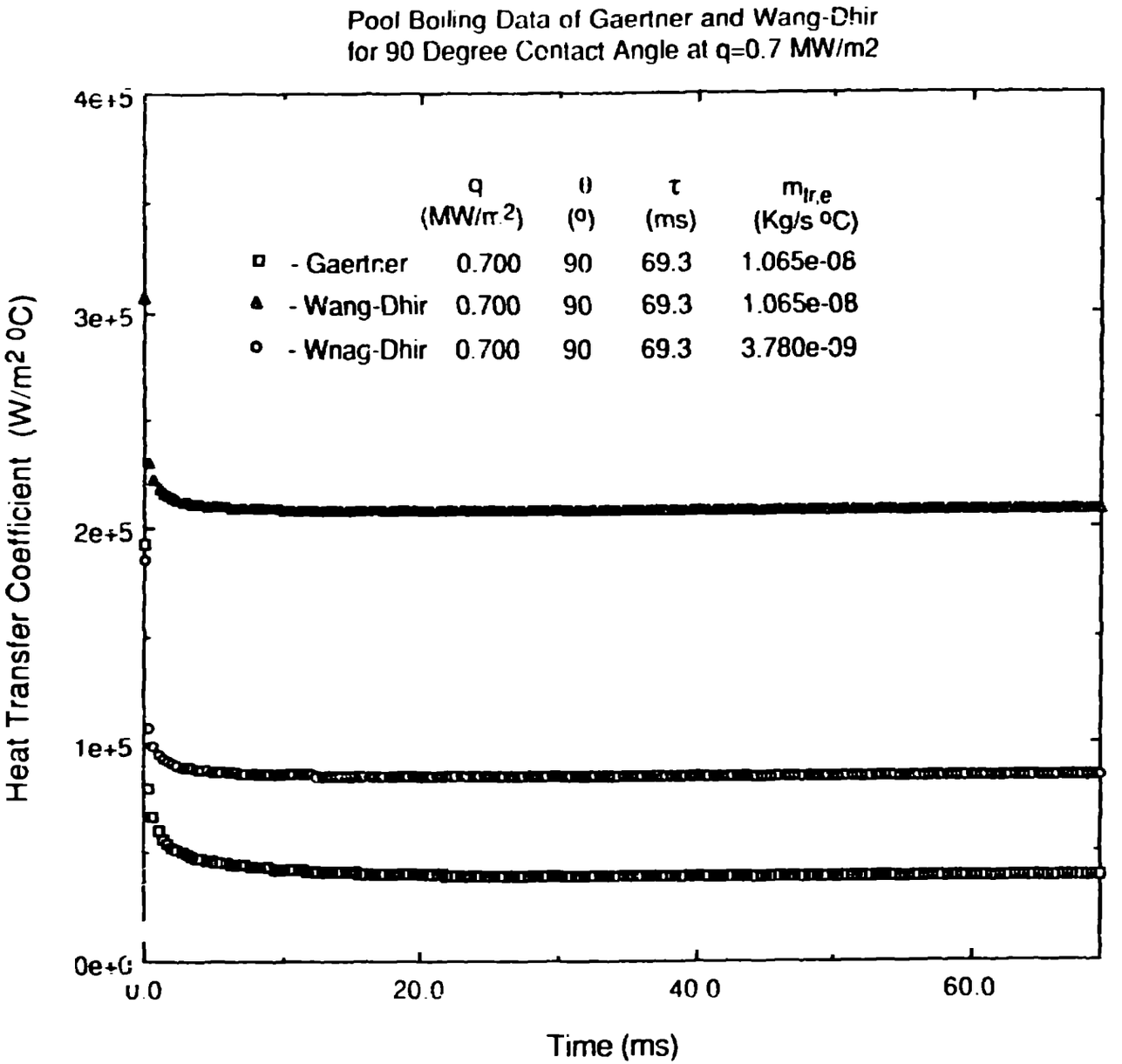

Fig. 9. Comparison of the surface-averaged transient heat-transfer coefficients in the two-phase macrolayer region for Gaertner's and Wang's and Dhir's 90° contact angle data.

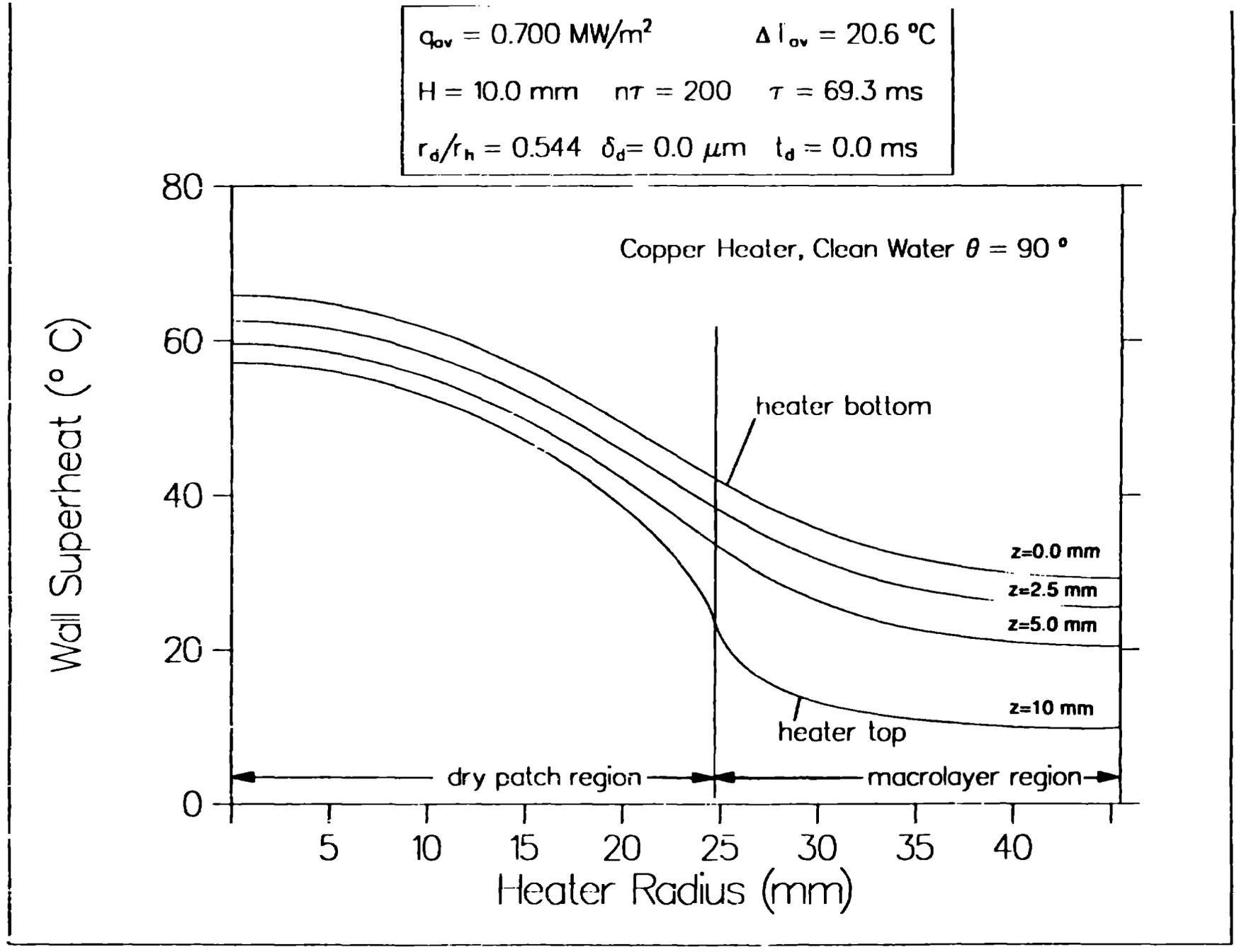

Fig. 10. The instantaneous radial wall temperature profiles at four different elevations at the end of converged hovering period for heat flux of 0.7 MW/m² and the evaporation coefficient of 3.78e-09 kg/°C- m-s for Wang's and Dhir's 90° contact angle data.